sciendo

POLISH MARITIME RESEARCH 4 (124) 2024 Vol. 31; pp. 122-130
10.2478/pomr-2024-0056

Stress Assessment of a Steel Bullet LPG Tank Under Differential Settlement Based on Geodetic Measurements and Sensitivity Analysis

Tomasz Ferenc*
Gdansk University of Technology, Faculty of Mechanical Engineering and Ship Technology, Poland
Rafał Gierasimczyk
Gdansk University of Technology, Faculty of Mechanical Engineering and Ship Technology, Poland
Tomasz Mikulski
Gdansk University of Technology, Faculty of Mechanical Engineering and Ship Technology, Poland

* Corresponding author: *tomasz.ferenc@pg.edu.pl (Tomasz Ferenc)*

ABSTRACT

This paper presents an analysis of a steel bullet LPG tank in operation at a base in Poland. The structure was set on a sand-gravel pillow and rigid concrete slab, and its settlement was periodically measured at five measuring points along the structure. After a few years, differential settlement was observed. Based on geodetic data, we attempt to assess the current stress level in the structure. The proposed methodology uses a sensitivity analysis apparatus. A numerical model of the structure and sand-gravel pillow is analysed using the finite element method, and the impact of variation in the stiffness of the sand-gravel pillow on the vertical displacement of the tank is determined. The algorithm involves six iterations of calculations, and after each iteration, the stiffness modified sand-gravel pillow is determined. After the sixth iteration, the vertical displacement in the FEM model is found to be similar to the measured values in the real structure. The results obtained after the last iteration are used to assess the stress state in the bullet tank's shell structure.

Keywords: LPG steel tank, stress assessment, sensitivity analysis, differential settlement

INTRODUCTION

The dynamic development of civilisation in the world has resulted in an increasing consumption of energy, and consequently an increasing demand for energy and raw materials. The tendency towards diversifying raw material supplies to achieve energy security for nations is becoming widespread [1]. Gas can be delivered via pipelines or transported, mainly by water, in liquefied form. In the latter case, infrastructure is necessary for storage.

Liquefied natural gas (LNG) storage bases [2] have been established at harbours worldwide, for example at Świnoujście Harbor in Poland [3]. These are usually cryogenic tanks where liquefied LNG gas is stored at temperatures ranging from –163 °C to –140 °C at a pressure of 4–5 bar (Fig. 1). These are cylindrical tanks with a vertical axis and large capacity. Due to the dimensions of the tanks, the foundation of the structure becomes extremely significant: incorrect structure support can lead to differential settlement [4] [5] [6] [7], which increases the stress levels in the structure [8].

Fig. 1. LNG storage base in Świnoujście, Poland (https://www.gaz-system.pl/pl/terminal-lng/informacje-o-terminalu-lng.html)

Another type of gas used in many economies is liquefied petroleum gas (LPG), which is mainly a by-product of crude oil refining [9] [10] [11]. The properties of LPG allow it to be stored in liquefied form at a temperature of approximately +40°C and a vapor pressure of approximately 16 bar. Such a high pressure requires a different tank design, and many factors must be taken into account, such as strength and stability [12], burst strength [13] [14], and buckling behavior [15] [16]. The maintenance of the tank is also significant [17]. Since the gas is flammable, the tank's behaviour under fire or explosion may also need to be analysed [18] [19]. LPG storage tanks, also known as bullet tanks, are usually steel cylindrical tanks with a horizontal axis, a diameter of 5.6–8 m, and a length of 70–100 m. In a similar way to the LNG tank, the foundation of the LPG tank is significant. An LPG tank is usually placed on a rigid reinforced concrete plate by a compacted sand-gravel ballast (pad), creating a system of several tanks placed next to each other. This foundation is intended to provide even support for the cylindrical shell of the tank, to eliminate any concentration of foundation reaction forces. The tank is also mounded to protect it against environmental impacts such as excessive sunlight. The mound is exposed to precipitation, and the water falling on the mound must be effectively drained from the sand and gravel via a drainage system. The irrigated soil loses its load-bearing capacity, and may result in differential settlement and additional stresses in the tank's structure.

Both types of tank are usually located in the port area, and are subject to supervision by the Maritime Office. Moreover, the gas stored in the tanks is delivered by gas carriers. Hence the design, manufacture, and maintanence of such structures are related to the broadly understood maritime economy.

In order to monitor the quality of the foundation of an LPG tank, measuring points can be installed above the tank. If the settlement measurements taken at these points change linearly along the tank, then the tank is settling uniformly without generating additional stresses; otherwise, a change in the tank geometry and generation of stresses in addition to those resulting from the action of the main load (i.e. a working pressure of up to 16 bar) should be expected. Both the mound and the hydrostatic pressure of the liquefied gas have a negligible impact on the stress state.

This study aims to assess the stress level in a real LPG tank structure located at a base in Poland, caused by measured differential settlement. We present an analysis of an actual tank in operation, for which settlement measurements are periodically performed at five measuring points (MPs). Of the several tanks in the system, the one with the highest differences in measured settlement was selected. An attempt is made to assess the stress level in the tank structure based on the measurement data collected during the use of the tank. Since the tank is covered with sand, the only available data consist of vertical displacements at five points located along the structure that protrudes above the ground surface. To assess the stress state of the bullet tank's shell structure, an inverse problem procedure is used, based on a sensitivity analysis apparatus [20] [21] [22] [23] [24]. In the analysis presented here, the stiffnesses of the sand-gravel pillow, which is divided into sections, are considered as the design variables that are subject to changes, while the settlement values at the measurement points are taken as the state variables. Based on the results, it is possible to estimate the stress level in the structure itself. This is important for safety reasons, since LPG is stored at high pressure. The results of this work and the analysis methodology can be used by a tank operator to assess the current stress level of the structure.

DESCRIPTION OF THE TANK

GEOMETRY AND MATERIAL

The bullet tank analysed here is a thin-walled steel structure with an overall length of 70.5 m and a diameter of 5.6 m (Fig. 2). The structure was placed on a sand-gravel pillow with compaction factor I_d = 0.97–1.00 and, below this was a foundation that consisted of a reinforced concrete slab based on drilled concrete piles. To drain water from under the tank, drainage pipes were installed. According to the designer's assumption, this solution should prevent differential settlement of the tank.

The entire cylindrical structure consists of 22 sections with a length of 2.95 m, which are connected by circumferential welding. The cylindrical shell is made of steel sheets 26 mm thick while the spherical heads (domes) are 25 mm thick. The structure is strengthened with circumferential ribs spaced 2.95 m apart, with one rib per segment. The ribs have

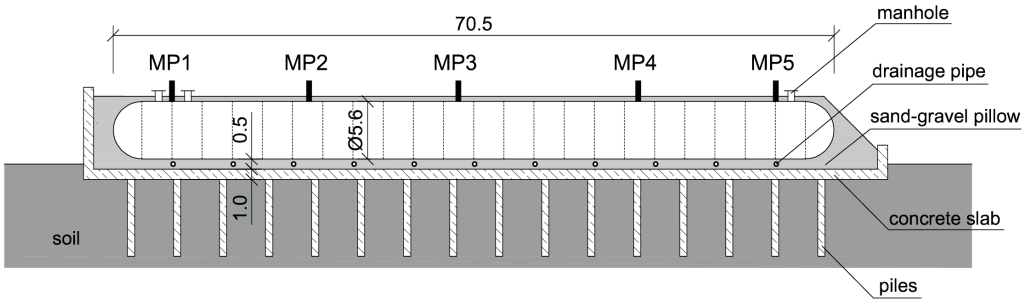

Fig. 2. Dimensions of the bullet tank [m]

a T-section (Fig. 3) with a web height of 305 mm and a flange width of 200 mm. Both flange and web are made of 26 mm thick steel sheets. The stiffening ribs are placed 300 mm from the edge of each section.

In addition, three manholes are located in the upper part of the tank body (see Fig. 2). All manholes have the same dimensions: the inner diameter is 679 mm, while the height is 600 mm. The walls of the manholes are made from 16 mm thick steel sheets. The upper part of the structure is stiffened by a steel collar with a diameter of 910 mm and a thickness of 50 mm. A 60 mm thick cover is screwed to the collar with 24 M33×155 bolts. Moreover, the manhole is strengthened with an overlay that is 20 mm thick and 1250 mm in diameter.

The tank is built from two types of structural steel. The cylindrical body, spherical heads, and manholes are made from S355 steel, and strengthened circumferential ribs are made from S235 steel. The material parameters are given in Table 1.

All data are taken from the tank's technical documentation.

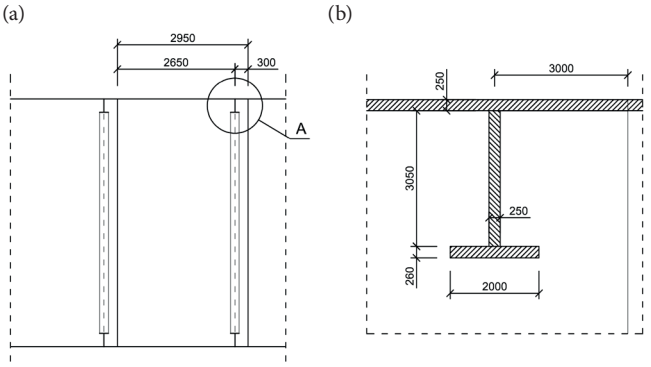

Fig. 3. Details of: (a) a segment of the tank, (b) a circumferential rib with a T-section [mm]

Tab. 1. Material parameters

Element	Steel	Parameter	Value	Description
Cylindrical body Spherical heads Manholes	S355	R_e	345 MPa	Yield point
		R_m	470 MPa	Strength
		E	210 GPa	Stiffness modulus
		ν	0.3	Poisson's ratio
Circumferential ribs	S235	R_e	225 MPa	Yield point
		R_m	340 MPa	Strength
		E	210 GPa	Stiffness modulus
		ν	0.3	Poisson's ratio

COMPUTATIONAL MODEL OF THE TANK AND SOIL

Description of the FEM model

The computational model was created in FEMAP with NX Nastran 10.1 commercial software using the finite element method (FEM). Due to its symmetry, only half of the structure was analysed. All structural parts were taken into account, including the main body of the tank, circumferential ribs, and manholes, and were modeled by means of four-node shell elements with linear shape functions and full integration.

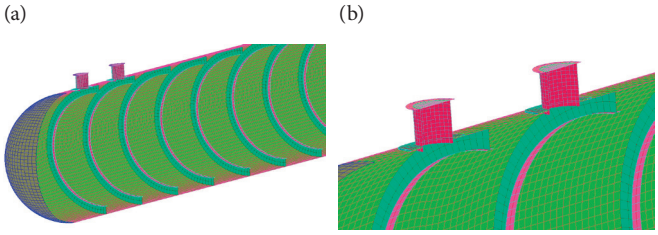

Fig. 4. FEM model of the tank: (a) overall view; (b) detail

Since the study focused on the impact of differential settlement on the stress level in the tank, the sand-gravel pillow was also taken into account. No topsoil load was assumed, so the backfill pressure was taken as negligible. Hence, only the zone that contained the tank foundations was taken into account. Moreover, it was assumed that the angle of support from the tank to the ground was 120°, as shown in Fig. 5a. The sand-gravel pillow was modeled using eight-node solid elements with linear shape functions and full integration, with a value of the elastic modulus E [GPa] that corresponded to the stiffness of the ground k [MN/m^3]. This approach is equivalent to the Winkler model for soil-structure interaction, according to elastic theory, and these assumptions were made because the soil structure itself was not the focus of the research. Furthermore, the structure was merged with the sand-gravel pillow by means of a "glue type" connection, where the tank was assumed to be an independent area (known as a "master") while the soil was a dependent one (known as a "slave"). An example of a this type of connection is presented in Fig. 5b.

After the convergence study of the mesh grid, the characteristic size of single finite elements was taken as 150 mm, giving total numbers of elements and nodes of 505,728 and 156,149, respectively.

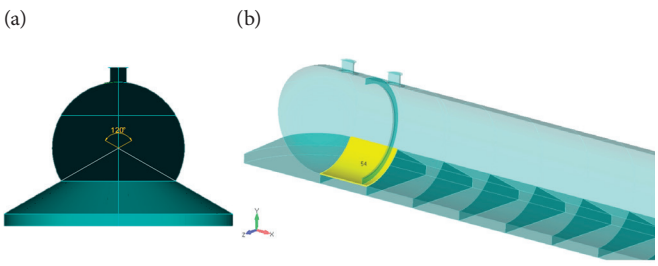

Fig. 5. Model of the tank supported by the sand-gravel pillow: (a) assumed angle of support; (b) connection between the tank and sand-gravel pillow

Boundary conditions

The exploitation pressure of the tank was 1.6 MPa. The hydrostatic pressure of the liquefied gas was also taken into account, and it was assumed that the density of liquefied LPG gas was 550 kg/m^3 and that liquid level was 4.46 m, equivalent to 85% of the tank diameter (height). The total pressure was then obtained according to the equation

$$p(y) = p_0 + \rho_{LPG} \cdot g \cdot y \quad (1)$$

where $p(y)$ is the total pressure [MPa], which varies along the height of the tank; p_0 is the exploitation pressure [MPa]; ρ_{LPG} is the mass density of liquefied LPG gas [kg/m^3]; $g = 9.81$ m/s^2 is the gravitational acceleration; and y is the depth of liquefied gas [m].

The dead load was taken into account, based on the assumption that the density of steel was equal to 8,000 kg/m^3. Due to structural symmetry, only half of it was analysed, and symmetrical boundary conditions were assumed in the plane of symmetry.

Results of a preliminary analysis of the tank

When carrying out a preliminary analysis of the tank, the loadings mentioned above were applied, i.e. the exploitation pressure, the hydrostatic pressure of liquefied gas, and the dead load. The initial value of the elastic modulus for the sand-gravel pillow was taken to be 20 MPa. For these conditions, the Huber-Mises-Hencky HMH (also known as von Mises) stress maps of the tank structure, both top and bottom, are presented in Fig. 6. The extreme value of stress obtained for the tank cylindrical shell was 151 MPa, while in the spherical heads and circumferential ribs, the stresses were at the level of 107 MPa and 112 MPa, respectively. However, the highest value of HMH stress occurred locally in the shell of the manholes, as shown in Fig. 7, and exceeded 330 MPa. Nowhere in the structure of the tank did the stress level exceed the yield point of the material.

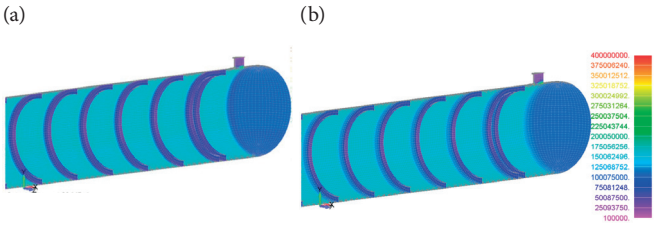

Fig. 6. HMH stress maps [Pa]: (a) top, (b) bottom

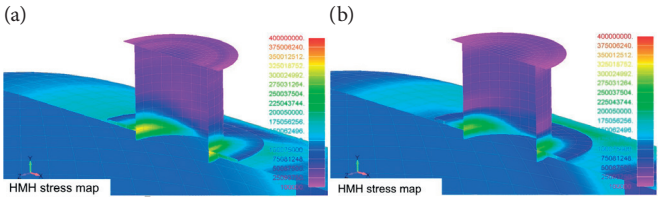

Fig. 7. HMH stress maps for the walls of the manholes [Pa]: (a) top; (b) bottom

Fig. 8 shows the stress levels in the sand-gravel pillow under the tank. It can be observed that the smallest stress value occurs under the circumferential ribs, and that the stress values increase from the mid-length to the end of the tank.

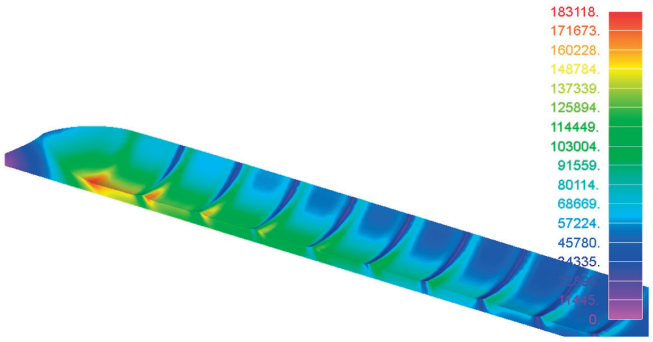

Fig. 8. Compression stress map of the sand-gravel pillow [Pa]

METHOD

EXPERIMENTAL STUDY OF DIFFERENTIAL SETTLEMENT OF THE TANK

When the tank had been constructed, five MPs were installed on its top, to control its vertical translations during the experiment (Fig. 9). The structure was placed on a very stiff reinforced concrete slab, and the settlement of this slab was also taken into account. However, due to its thickness of 1 m, the slab was considered as a rigid body, and the difference between the vertical settlement of the concrete foundation and the tank caused differential settlement that impacted the tank structure. After interpolation of the measured values of vertical displacement of the concrete slab at the MPs, we obtained relative values of the vertical settlement that was equivalent to the assumed differential settlement, as listed in Table 2.

It can be seen that there was differential settlement along the tank. We can therefore assume that the stress level in the structure is different from the initial calculations, due to this differential settlement. Hence, in the next part of the paper, the influence of the soil settlement on the structure was analysed.

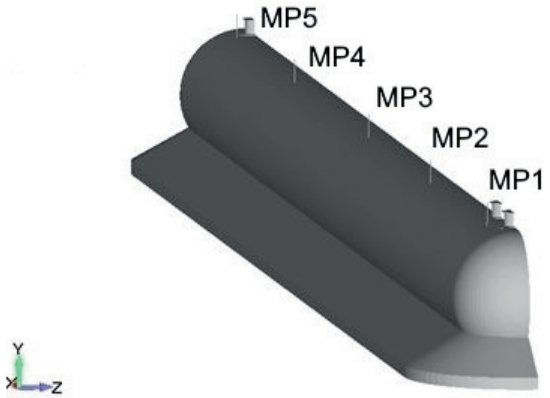

Fig. 9. Locations of measuring points

Tab. 2. Assumed relative displacements obtained at measuring points (MPs)

Measuring point	Vertical displacement [mm]		
	Measured value at measuring point	Interpolated value of settlement of concrete slab	Relative vertical displacement
MP1	79	18.1	60.9
MP2	60	22.6	37.4
MP3	48	25.9	22.1
MP4	41	26	15.0
MP5	39	28.4	10.6

REVERSE PROBLEM PROCEDURE

The measured differential settlement of the tank was assumed to be caused by variations in the stiffness of the sand-gravel pillow. In order to simulate this, the pillow in the FEM model was divided into 13 sections along the length, as shown in Fig. 10. Each section could be described by a different elastic modulus E_i, and to determine these values, a reverse problem procedure was conducted.

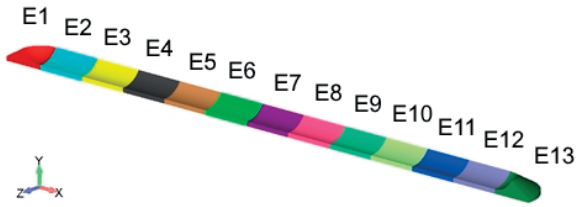

Fig. 10. Sections of the sand-gravel pillow under the tank

Assessing the stiffness distribution along the length of the tank involved finding values for the elastic modulus E_i (i = 1,2,…,13) that would give displacements at the MPs in the numerical analysis with values closest to those measured. The objective function used in the procedure was expressed by the least squares method, and took into account the differences in displacements between the real tank and the FEM model. The objective function for which the minimum was determined was defined as

$$F = \sum_{j=1}^{5}\left[\overline{u}_j - \left(u_j + du_j\right)\right]^2 \tag{2}$$

where $\overline{u}_j$ is the displacement at the j-th measuring point (j = 1,2,…,5) of the real tank; u_j is the displacement at the j-th measuring point in the FEM model; and du_j is the unknown value of the variation in the displacement at the j-th measuring point in the FEM model for which the function reaches a minimum.

Furthermore, the relation between the displacement at the j-th MP in the FEM model caused by the variation in the sand-gravel pillow stiffness (expressed by the elastic modulus δE_i) is described by the application of linear sensitivity coefficients $w_{i,j}$. To compute these, the initial values of the elastic moduli have to be assumed, as follows:

$$\left[E_i^{\,0}\right] = \begin{bmatrix} E_1^{\,0} \\ E_2^{\,0} \\ \cdots \\ \cdots \\ E_{12}^{\,0} \\ E_{13}^{\,0} \end{bmatrix} \tag{3}$$

and the initial displacement in the j-th MP is determined as

$$\left[u_j^{\,0}\right] = \left[u_1^{\,0} \quad u_2^{\,0} \quad u_3^{\,0} \quad u_4^{\,0} \quad u_5^{\,0}\right]^T \tag{4}$$

Then, to find the sensitivity coefficients $w_{i,j}^{\,k}$, a series of computations was conducted, where k represents the step of the process (k = 1,2,…,5). The elastic modulus in each section was decreased by 10% $\left(E_i^k = 0.9E_i^{k-1}\right)$, and the displacement in each measuring point was computed:

$$\left[u_{i,j}^{\,k}\right] = \left[u_{i,1}^{\,k} \quad u_{i,2}^{\,k} \quad u_{i,3}^{\,k} \quad u_{i,4}^{\,k} \quad u_{i,5}^{\,k}\right]^T \tag{5}$$

Then, based on the results, the linear sensitivity coefficients were computed as

$$w_{i,j}^{\,k} = \frac{u_j^{\,k} - u_{i,j}^{\,k-1}}{E_i^k - E_i^{k-1}} \tag{6}$$

and were listed in the sensitivity vectors as follows:

$$\left[w_{i,1}^{\,k}\right] = \begin{bmatrix} w_{1,1}^{\,k} \\ w_{2,1}^{\,k} \\ \cdots \\ w_{12,1}^{\,k} \\ w_{13,1}^{\,k} \end{bmatrix} \quad \left[w_{i,2}^{\,k}\right] = \begin{bmatrix} w_{1,2}^{\,k} \\ w_{2,2}^{\,k} \\ \cdots \\ w_{12,2}^{\,k} \\ w_{13,2}^{\,k} \end{bmatrix} \quad \left[w_{i,3}^{\,k}\right] = \begin{bmatrix} w_{1,3}^{\,k} \\ w_{2,3}^{\,k} \\ \cdots \\ w_{12,3}^{\,k} \\ w_{13,3}^{\,k} \end{bmatrix} \quad \left[w_{i,4}^{\,k}\right] = \begin{bmatrix} w_{1,4}^{\,k} \\ w_{2,4}^{\,k} \\ \cdots \\ w_{12,4}^{\,k} \\ w_{13,4}^{\,k} \end{bmatrix} \quad \left[w_{i,5}^{\,k}\right] = \begin{bmatrix} w_{1,5}^{\,k} \\ w_{2,5}^{\,k} \\ \cdots \\ w_{12,5}^{\,k} \\ w_{13,5}^{\,k} \end{bmatrix} \tag{7}$$

Thus, the objective function could be expressed in terms of the sensitivity coefficients as follows:

$$F = \sum_{j=1}^{5}\left[\overline{u}_j - \left(u_j^{\,k} + \left[w_{i,j}^{\,k}\right]^T \cdot \left[\delta E_i^{\,k}\right]\right)\right]^2 \tag{8}$$

where the unknown value $\delta E_i^{\,k}$ that is sought is the value of the variation of elastic modulus in each i-th soil section after the k-th iteration. The objective functions can be also expressed in terms of the relative values as:

$$F = \sum_{j=1}^{5}\left[\frac{\bar{u}_j}{u_j^k} - \left(\frac{u_j^k}{u_j^k} + \frac{\left[w_{i,j}^k\right]^T E_i^k}{u_j^k} \cdot \left[\frac{\delta E_i^k}{E_i^k}\right]\right)\right]^2 = \sum_{j=1}^{5}\left[\tilde{u}_j - \left(1 + \left[\tilde{w}_{i,j}^k\right]^T \cdot \left[\delta \tilde{E}_i^k\right]\right)\right]^2 \quad (9)$$

The objective function is in the form of a least squares function, and its minimum is sought at the k-th iteration step. This allows us to determine the relative variations in the elastic modulus of the sand-gravel pillow in the i-th section $\delta \tilde{E}_i^k$ and then to modify its stiffness for the next iteration step.

RESULTS AND DISCUSSION

RESULTS OF THE REVERSED PROBLEM

The reverse problem procedure was conducted to determine the elastic moduli E_i^k in each sand-gravel pillow segment according to Eqs. (3)–(9). At the beginning, an initial step (Step 0) was conducted in which the initial values of elastic moduli were assumed, as listed in Table 3. For these values, the initial values of displacement in the measuring points were computed as listed in Table 4. Then, five iterations were performed, until the relative error between the computed points and MPs was less than 2%. In each iteration, the sensitivity coefficients $w_{i,j}^k$ were determined according to Eq. (6) after the elastic modulus in each segment had been decreased by 10% and the displacements at the MPs $u_{i,j}^k$ had been computed. Following this, the minimum of the objective function was determined to find the desired foundation segment variations δE_i^k. In the first iteration, the elastic moduli could take values in the range –99% to +10% of the initial values, while in the following iterations, the values could vary from –60% to +60%. As a result, after each iteration, the new values of elastic moduli E_i^k were determined as listed in Table 3, and the new displacements at the MPs u_j^k were also computed as shown in Table 4. In Table 4, the measured values of the displacements at the MPs are also presented for comparison, together with the computed relative error between each result and the value obtained after the last (fifth) iteration, according to the equation

$$\Delta u_j = \frac{\left(\bar{u}_j - u_j^5\right)}{\bar{u}_j} \quad (10)$$

The results after each iteration are also presented graphically in Fig. 11 for the elastic moduli and in Fig. 12 for the displacements at the MPs.

Tab. 3. Values of the elastic modulus after each iteration

	Elastic modulus [kPa]					
	Initial step (0)	After the k-th iteration				
		1	2	3	4	5
E_1	500	5	8	13	5	2
E_2	500	5	8	13	5	2
E_3	500	5	8	13	5	2
E_4	500	42	68	108	44	19
E_5	1000	1.100	1.760	2.816	3.098	2.708
E_6	1000	1.100	1.760	1.270	2.030	3.244
E_7	1000	1.100	440	176	135	117
E_8	1500	1.650	660	264	107	46
E_9	1500	1.650	2.293	917	369	150
E_{10}	1500	1.650	2.640	3.434	2.065	832
E_{11}	2000	775	1.241	1.985	3.174	4.056
E_{12}	2000	20	32	51	81	127
E_{13}	2000	20	32	51	81	124

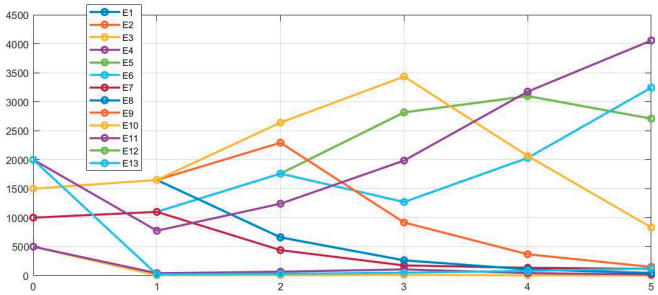

Fig. 11. Values of the elastic modulus after each iteration

Tab. 4. Displacements at the measuring points after each iteration

	Displacement at measuring points [mm]							Relative error
	Initial step (0)	After the k-th iteration					Measured	
		1	2	3	4	5		
u_1	33	103	80	66	61	60	61	2.0%
u_2	27	64	50	42	39	38	37	1.8%
u_3	21	32	25	24	23	22	22	0.9%
u_4	13	15	13	15	15	15	15	1.3%
u_5	6	10	10	10	11	11	11	1.1%

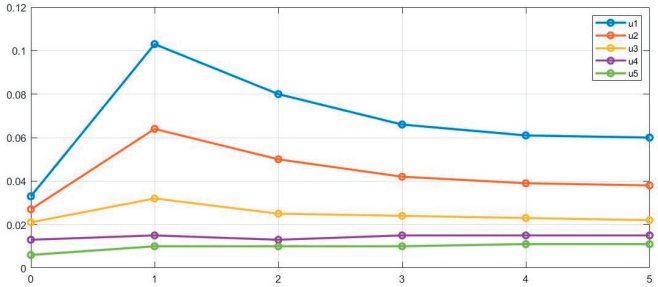

Fig. 12. Displacements at the measuring points after each iteration

RESULTS OF THE ANALYSIS OF THE TANK

After this procedure, the final values of the elastic moduli were computed and used in the FEM model (see the last column in Table 3). The dead load and exploitation pressure were applied to the structure as described above.

This analysis allowed us to determine the displacement of the structure as well as the stress levels in the tank due to differential settlement. Fig. 13 shows the deformation of the tank, multiplied 20 times. It can be observed that the tank was bent between the sixth and eighth circumferential ribs; the tank became oval due to this effect, and the horizontal displacement in that area reached about 6.5 mm, as shown in Fig. 14.

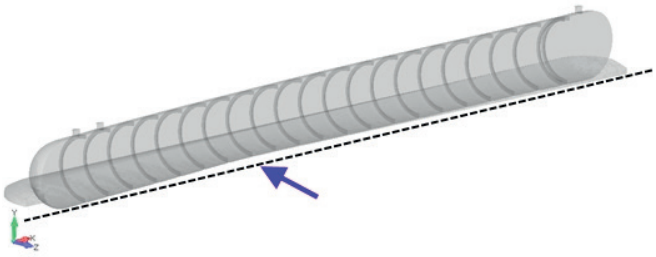

Fig. 13. Deformation of the tank under differential settlement (magnified 20 times)

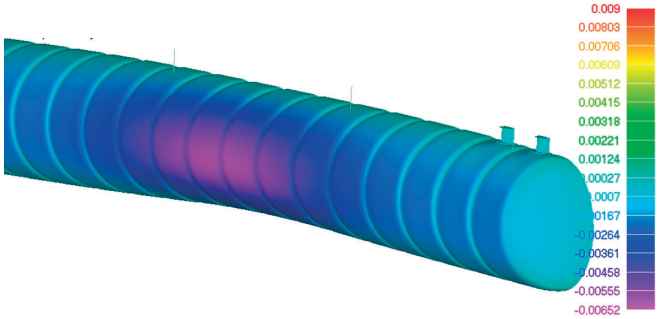

Fig. 14. Horizontal deformation of the tank [m]

The HMH stresses in the structure were determined and are presented in the form of stress maps in Fig. 15 and Fig. 16.

As can be observed, the level of stress in each structural element is constant except between the sixth and tenth circumferential ribs, where the values are higher than in the others. This corresponds to the area in which the tank is bent (see Fig. 13). However, the stress level in the cylindrical body is not increased in this zone.

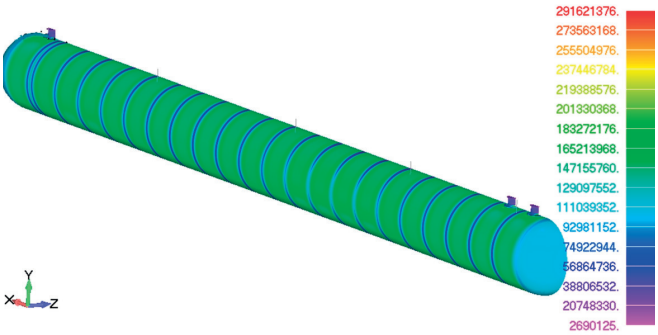

Fig. 15. HMH stress map on the outer shell surface

The extreme values of the HMH stress in each structural element are listed in Table 5, and are compared with the values obtained without taking into account differential settlement.

Tab. 5. Comparison of stresses in each structural element

Structural element	Without differential settlement		With differential settlement		Comparison
	HMH stress [MPa]	Compared to yield point	HMH stress [MPa]	Compared to yield point	
Cylindrical body	151.4	43.88%	156.2	45.28%	3.17%
Dome	107	31.01%	107.3	31.10%	0.28%
Ribs (flange)	112.9	50.18%	211.5	94.00%	87.33%
Ribs (web)	94.5	42.00%	212.5	94.44%	124.87%

Due to differential settlement, an extreme value of the stress in the circumferential ribs was was obtained as 212.5 MPa. It should be emphasised that the value was increased by nearly 124% from the value of 94.5 MPa obtained via the FEM model without taking into account the differential settlement. Moreover, the stress values obtained for the

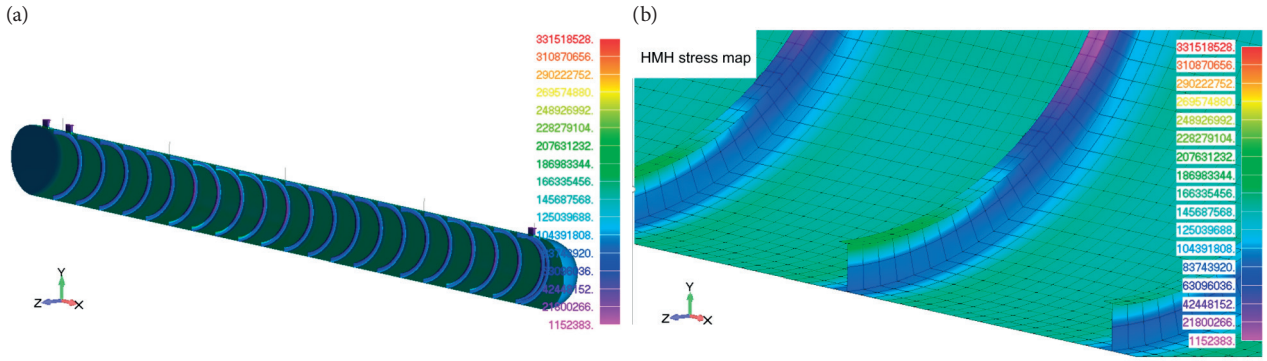

Fig. 16. HMH stress maps on the out

cylindrical body and dome, with and without differential settlement, did not increase significantly (less than 3%). Thus, differential settlement causes an increase in stress levels, and mainly in the circumferential ribs.

As discussed above, the stress level did not exceed the yield point of the material anywhere in the structure of the tank. However, a stress level of about 95% compared to the yield point may be considered a threat to the safety of the structure.

CONCLUSION

The analysis presented in this paper shows that periodic monitoring of the settlement of the LPG tank provides valuable data that allow us to assess whether differential settlement may result in an unsafe stress level in the structure. This is very important, especially in the case of high-risk facilities such as fuel reloading terminals for tanks.

The reverse problem procedure that was applied in this study allowed us to obtain values for the tank displacement measured at the MPs that were close to those in the FEM model. After five iterations, the relative error between the measured and computed displacements was less than 2%.

A simple sand-gravel pillow model of the Winkler type was adopted for these calculations. The aim of the study was not to identify the states of deformation and stress of the soil itself, but to assess its stiffness, in order to obtain the best accuracy for the displacement measured at the MPs for the real tank and the numerical model. On this basis, it was possible to assess the state of deformation and stress in the tank structure.

The analysis performed here allowed us to evaluate the stress levels in the individual elements of the tank. As discussed above, nowhere did the stress level exceed a level that could be dangerous for the structure. The proposed procedure for assessing the stress level in the structure may be used in the future in cases of differential settlement increases. Performing the iterative procedure presented here with updated measured geodetic data and FEM analyses can allow us to assess the stress levels in the structure at each moment.

Based on these analyses, it can be concluded that it is highly probable that LPG tanks (or bullet tanks) will settle differentially during operation. In order to minimise this differential settlement, it is necessary to preserve the sand-gravel pillow, for example by properly installing and maintaining drainage systems so that the water is evenly drained from under the tank.

The work presented in this paper formed part of an engineering project.

REFERENCES

1. Gritz A, Wolff G. Gas and energy security in Germany and central and eastern Europe. Energy Policy 2024. https://doi.org/10.1016/j.enpol.2023.113885.
2. Calderón M, Illing D, Veiga J. Facilities for bunkering of liquefied natural gas in ports. Transp. Res. Procedia 2016. https://doi.org/10.1016/j.trpro.2016.05.288.
3. Zarzecki D. Development of the LNG terminal in Świnoujście, Poland. In: The future of energy consumption, security and natural gas. Springer International Publishing, Cham; 2022; pp. 191–220. https://doi.org/10.1007/978-3-030-80367-4_7.
4. Cao Q, Zhao Y. Buckling strength of cylindrical steel tanks under harmonic settlement. Thin-Walled Struct. 2010. https://doi.org/10.1016/j.tws.2010.01.011.
5. Gong J-G, Zhou Z-Q, Xuan F-Z. Buckling strength of cylindrical steel tanks under measured differential settlement: Harmonic components needed for consideration and its effect. Thin-Walled Struct. 2017. https://doi.org/10.1016/j.tws.2017.06.020.
6. Zhao Y, Lei X, Wang Z, Cao Q. Buckling behavior of floating-roof steel tanks under measured differential settlement. Thin-Walled Struct. 2013. https://doi.org/10.1016/j.tws.2013.04.015.
7. Grget G, Ravnjak K, Szavits-Nossan A. Analysis of results of molasses tanks settlement testing. Soils Found. 2018. https://doi.org/10.1016/j.sandf.2018.07.009.
8. Ignatowicz R, Hotala E. Failure of cylindrical steel storage tank due to foundation settlements. Eng. Fail. Anal. 2020. https://doi.org/10.1016/j.engfailanal.2020.104628.
9. Sobczyk B. LNG Tank in Świnoujście: Nonlinear Analysis of the Tank Dome Elements Behaviour. Polish Maritime Research. 2020. https://doi.org/10.2478/pomr-2020-0074
10. An Sy, Jeong Hw, Kim O, Jaewoo Shim W. Effects of Sway and Roll Excitations on Sloshing Loads in a KC-1 Membrane LNG Tank. Polish Maritime Research. 2023. https://doi.org/10.2478/pomr-2023-0057
11. Bao G, Qin W, Jiang Q, Pu C. Study of Predictive Control Model for Cooling Process of Mark III LNG Bunker. Polish Maritime Research. 2024. https://doi.org/10.2478/pomr-2024-0040
12. Błachut J, Magnucki K. Strength, stability, and optimization of pressure vessels: Review of selected problems. Appl. Mech. Rev. 2008. https://doi.org/10.1115/1.2978080.
13. Johnson W R, Zhu X-K, Sindelar R, Wiersma B. A parametric finite element study for determining burst strength of thin and thick-walled pressure vessels. Int. J. Press. Vessel. Pip. 2023. https://doi.org/10.1016/j.ijpvp.2023.104968.

14. Kuanhai D, Yuanhua L, Bing L, Xiaohong W. Investigation on the calculation model of burst pressure for tube and casing under practical service environment. Int. J. Hydrogen Energy 2019. https://doi.org/10.1016/j.ijhydene.2019.06.205.

15. Burgos C A, Jaca R C, Godoy L A. Post-buckling behavior of fluid-storage steel horizontal tanks. Int. J. Press. Vessel. Pip. 2018. https://doi.org/10.1016/j.ijpvp.2018.03.001.

16. Magnucki K, Jasion P, Rodak M. Strength and buckling of an untypical dished head of a cylindrical pressure vessel. Int. J. Press. Vessel. Pip. 2018. https://doi.org/10.1016/j.ijpvp.2018.02.003.

17. De-León-Escobedo D. Risk-based maintenance time for oil and gas steel pipelines under corrosion including uncertainty on the corrosion rate and consequence-based target reliability. Int. J. Press. Vessel. Pip. 2023. https://doi.org/10.1016/j.ijpvp.2023.104927.

18. Luo W, Bi M, Yu D, Deng Z, Sun S, Ren J. A damage mechanics model under dynamic thermal loads and its application to pressure vessels under fire invasion. Eng. Fract. Mech. 2024. https://doi.org/10.1016/j.engfracmech.2024.110011.

19. Bradley I, Scarponi G E, Otremba F, Birk A M. An overview of test standards and regulations relevant to the fire testing of pressure vessels. Process Saf. Environ. Prot. 2021. https://doi.org/10.1016/j.psep.2020.07.047.

20. Barthelemy B, Chon C T, Haftka R T. Accuracy problems associated with semi-analytical derivatives of static response. Finite Elem. Anal. Des. 1988. https://doi.org/10.1016/0168-874X(88)90011-X.

21. Bletzinger K-U, Firl M, Daoud F. Approximation of derivatives in semi-analytical structural optimization. Comput. Struct. 2008. https://doi.org/10.1016/j.compstruc.2007.04.014.

22. De Boer H, van Keulen F. Refined semi-analytical design sensitivities. Int. J. Solids Struct. 2000. https://doi.org/10.1016/S0020-7683(99)00322-4.

23. Ferenc T. Multiparameter sensitivity analysis of a GFRP composite footbridge of a sandwich structure and u-shaped cross-section. Compos. Struct. 2020. https://doi.org/10.1016/j.compstruct.2020.112793.

24. Kiendl J, Schmidt R, Wüchner R, Bletzinger K-U. Isogeometric shape optimization of shells using semi-analytical sensitivity analysis and sensitivity weighting. Comput. Methods Appl. Mech. Eng. 2014. https://doi.org/10.1016/j.cma.2014.02.001.